

An experimental study of a bio-inspired corrugated airfoil for micro air vehicle applications

Jeffery T. Murphy · Hui Hu

Received: 13 July 2009/Revised: 13 January 2010/Accepted: 13 January 2010/Published online: 4 February 2010
© Springer-Verlag 2010

Abstract An experimental study was conducted to investigate the aerodynamic characteristics of a bio-inspired corrugated airfoil compared with a smooth-surfaced airfoil and a flat plate at the chord Reynolds number of $Re_C = 58,000$ – $125,000$ to explore the potential applications of such bio-inspired corrugated airfoils for micro air vehicle designs. In addition to measuring the aerodynamic lift and drag forces acting on the tested airfoils, a digital particle image velocimetry system was used to conduct detailed flowfield measurements to quantify the transient behavior of vortex and turbulent flow structures around the airfoils. The measurement result revealed clearly that the corrugated airfoil has better performance over the smooth-surfaced airfoil and the flat plate in providing higher lift and preventing large-scale flow separation and airfoil stall at low Reynolds numbers ($Re_C < 100,000$). While aerodynamic performance of the smooth-surfaced airfoil and the flat plate would vary considerably with the changing of the chord Reynolds numbers, the aerodynamic performance of the corrugated airfoil was found to be almost insensitive to the Reynolds numbers. The detailed flow field measurements were correlated with the aerodynamic force measurement data to elucidate underlying physics to improve our understanding about how and why the corrugation feature found in dragonfly wings holds aerodynamic advantages for low Reynolds number flight applications.

1 Introduction

The concept of micro-sized unmanned aerial vehicles (UAVs) or micro air vehicles (MAVs) has gained increasing interest over the past few years, with the principal aim of carrying out surveillance missions. MAVs typically refer to palm-sized aircraft with a maximal dimension on the order of 15 cm and a flight speed of about 10 m/s. The combination of small length scale and low flight speed results in a flight regime with very low Reynolds number. It has been found that the aerodynamic performances of a streamlined airfoil optimized for traditional macroscale aircraft at high Reynolds numbers would degrade significantly as the Reynolds number is reduced (Carmichael 1981; Lissaman 1983; Gad-el-Hak 2001). As a result, MAVs with conventional streamlined airfoil designs usually have quite poor aerodynamic performances, which limit their flight agility and versatility (Mueller 2001). Therefore, it is very necessary and important to establish novel airfoil design paradigms for MAV applications in order to achieve better aerodynamic performances for improved flight agility and versatility.

A number of insects including locusts, dragonflies and damselflies employ wings that are not smooth or simple cambered surfaces. The cross-sections of the wings have well-defined corrugated configurations (Rees 1975a; Kesel et al. 1998; Kesel 2000). The corrugated configuration was found to be of great importance to provide stiffening against spanwise bending, while allowing for torsion and the development of camber (Rees 1975b; Newman et al. 1977). The corrugated wings are also found to be structurally stabilized primarily by the folded configurations, which increases flexural rigidity to handle the spanwise bending forces and mechanical wear that the wing experiences during flapping (Rees 1975a, b; Sudo and Tsuyuki 2000).

J. T. Murphy · H. Hu (✉)
Department of Aerospace Engineering, Iowa State University,
Ames, IA 50011, USA
e-mail: huhui@iastate.edu

The corrugated wing configuration does not resemble a typical engineered airfoil, and does not appear to be suitable for flight since it would have very poor aerodynamic performance (i.e., low lift and extremely high drag) according to traditional airfoil design principles. However, several studies on corrugated dragonfly wings in steady flow or gliding flight (Rudolph 1977; Soms and Luttgies 1985; Azuma and Watanabe 1988; Okamoto et al. 1996; Wakeling and Ellington 1997; Kesel 2000; Thomas et al. 2004; Luo and Sun 2005; Vargas et al. 2008) have led to a surprising conclusion: a corrugated dragonfly wing could have comparable or even better aerodynamic performances (i.e., higher lift and bigger lift-to-drag ratio) compared with conventional smooth-surfaced airfoils in the low Reynolds number regime where dragonflies usually fly.

A number of hypotheses have been suggested to explain the fundamental mechanism of the rather unexpected aerodynamic performance improvement of corrugated dragonfly airfoils or wings over conventional smooth airfoils. By conducting wind tunnel experiments with scaled corrugated wing models, Rees (1975b) and Rudolph (1977) suggested that fluid flowing over the corrugated airfoil would be trapped between the corrugation valleys where it either becomes stagnant or rotates slowly, resulting in the corrugated airfoil functioning as a streamlined airfoil. Newman et al. (1977) suggested that the improved aerodynamic performance would be associated with the earlier reattachment of the flow separation on the corrugated wings. As the angle of attack increases, airflow would separate from the leading edge to form a separation bubble, and the separated flow would reattach sooner due to the corrugation compared with smooth airfoils. Rudolph (1977) also found that, compared with a streamlined technical airfoil, the tested corrugated airfoil would delay flow separation at higher angles of attack, and a stall did not occur abruptly. Based on filming free gliding dragonflies and conducting wind tunnel experiments on their wings at a chord Reynolds number ranging from 700 to 2,400, Wakeling and Ellington (1997) stated that the enhanced lift produced by corrugated dragonfly wings is not attributed to the Reynolds number, the aspect ratio or the wing area, but rather a surface feature, mainly the corrugations found in dragonfly wings. Based on detailed experiments to investigate the aerodynamic characteristics of dragonfly wings and model wings at a Reynolds number ranging from 11,000 to 15,000, Okamoto et al. (1996) also found that the corrugated wing model outperformed the flat plate at all angles of attack. The lift produced by a dragonfly wing was found to be higher than that produced by streamlined airfoils. Based on pressure measurements on the surfaces of a dragonfly wing model in addition to total lift and drag force measurements at a chord Reynolds number of 10,000, Kesel (2000) suggested that negative

pressure would be produced at the valleys of the corrugated dragonfly wing models, which would contribute to the increased lift. More recently, Luo and Sun (2005) and Vargas et al. (2008) conducted numerical studies to investigate the flow behaviors around corrugated dragonfly wings. Their simulation results confirmed that corrugated dragonfly wings would perform (in terms of the lift-to-drag ratio) as well and sometimes slightly better than smooth technical airfoils. The existence of small vortex structures in the valleys of the corrugated dragonfly airfoils were revealed clearly from the simulation results. The small vortex structures in the valleys of the corrugated cross-section were also revealed qualitatively in the flow visualization experiments of Kwok and Mittal (2005).

Despite different explanations about the fundamental mechanism for the improved aerodynamic performance, most of the studies agree that corrugated dragonfly airfoils or wings work well in low Reynolds number regimes, which naturally point to the potential applications of employing such corrugated airfoils or wings for MAV designs. With this in mind, we conducted the present study to try to leverage the corrugation feature of dragonfly wings and to explore the potential applications of such non-traditional, bio-inspired corrugated airfoils to MAV designs for improved aerodynamic performance.

It should be noted that, although a number of experimental studies have already been conducted previously to investigate the aerodynamic performance of corrugated dragonfly airfoils or wings, majority of previous studies on dragonfly wings or modeled corrugated airfoils were conducted from a biologist point of view to try to understand the fundamental mechanism of dragonfly flight mechanics. Therefore, the chord Reynolds number level of those studies is usually relatively small (i.e., $Re_C < 10,000$). The present study is conducted from the view point of an aerospace engineer to explore the potential applications of such non-traditional, bio-inspired corrugated airfoils in MAV designs. Thus, we chose to conduct the present study at the chord Reynolds number of $Re_C = 58,000\text{--}125,000$, i.e., in the range where MAVs usually operate, which is much higher than those previous experiments to study dragonfly flight aerodynamics.

In the present study, we report a comprehensive experimental investigation to quantify the aerodynamic characteristics of a bio-inspired corrugated airfoil, compared with a smooth-surfaced airfoil and a flat plate in the low Reynolds numbers range where MAVs usually operate. The experimental investigation was performed by using a low-speed wind tunnel. In addition to measuring total aerodynamic force (drag and lift) acting on the tested models, a digital particle image velocimetry (PIV) system was used to make detailed flowfield measurements to quantify the evolution of the unsteady vortex and turbulent

structures around the tested airfoils. The detailed flow field measurements are correlated with aerodynamic force measurements to elucidate underlying fundamental physics to explore/optimize design paradigms for the development of novel, bio-inspired corrugated airfoils for MAV applications.

It should also be noted that, our first report on this effort was made by Hu and Tamai (2008) to compare the aerodynamic performances of a bio-inspired corrugated airfoil, a NASA low-speed GA(W)-1 airfoil and a flat plate at the chord Reynolds number of $Re_C = 34,000$. The present work covers much wider and higher Reynolds number ranges ($Re_C = 58,000$ – $125,000$) to quantify the effects of Reynolds number on the aerodynamic performances of the bio-inspired corrugated airfoil for MAV applications. Furthermore, the airfoil thickness and the mean camber profile of the bio-inspired corrugated airfoil used by Hu and Tamai (2008) are different from those of the NASA low-speed GA(W)-1 airfoil, which can cause ambiguities in making direct comparisons of the aerodynamic performances of the airfoils. In the present study, the studied bio-inspired corrugated airfoil and smooth-surfaced technical airfoil have exactly the same mean camber profile and effective airfoil thickness, which will eliminate the ambiguities due to the effects of airfoil thickness and mean camber profile on the aerodynamic performances of the tested airfoils/wings.

2 Experimental setup and studied wings

The experimental study was conducted in a closed-circuit low-speed wind tunnel located in the Aerospace Engineering Department of Iowa State University. The tunnel has a test section with a 1.0×1.0 ft (30×30 cm) cross-section, and the walls of the test section are optically transparent. The tunnel has a contraction section upstream of the test section with honeycombs, screen structures and a cooling system installed ahead of the contraction section to provide uniform low turbulent incoming flow into the test section.

Figure 1 depicts the three airfoils used in the present study: a bio-inspired corrugated airfoil, a smooth-surfaced technical airfoil (i.e., profiled airfoil) and a flat plate airfoil. The cross-section of the bio-inspired corrugated airfoil corresponds to a typical cross-section of a dragonfly wing, which was digitally extracted from the profile given in Vargas and Mittal (2004) and has similar corrugation feature as the cross-section at the mid span of a corrugated dragonfly wing given in Kesel (2000). The coordinates of the corrugation corners of the bio-inspired corrugation airfoils are listed in Table 1, which are the measured values of the test model used in the present study. As shown

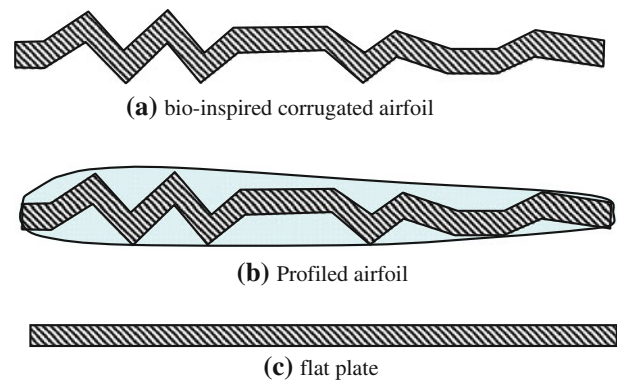


Fig. 1 The test airfoils

Table 1 The coordinates of the corrugation corners of the bio-inspired corrugated airfoil

Number of points	Upper surface		Number of points	Lower surface	
	X/C	Y/C		X/C	Y/C
1	0.000	0.020	1	0.000	-0.020
2	0.066	0.020	2	0.080	-0.020
3	0.124	0.058	3	0.128	0.010
4	0.189	0.016	4	0.187	-0.029
5	0.271	0.073	5	0.272	0.023
6	0.341	0.013	6	0.337	-0.036
7	0.398	0.051	7	0.415	0.014
8	0.553	0.051	8	0.537	0.014
9	0.610	0.015	9	0.606	-0.027
10	0.689	0.043	10	0.688	0.001
11	0.772	0.014	11	0.770	-0.028
12	0.833	0.010	12	0.839	-0.032
13	0.897	0.036	13	0.912	-0.005
14	1.005	0.020	14	0.995	-0.020

schematically in Fig. 1, the bio-inspired corrugated airfoil use in the present study has sharp edges at the corrugation corners. The smooth-surfaced technical airfoil was formed by tautly wrapping a thin film around the bio-inspired corrugated airfoil, which is similar as to form an “envelope” profile by fitting a spline through the protruding corners of the corrugated cross-section, in order to produce a smooth-surfaced airfoil. The flat plate has a rectangular cross-section with no rounding at the leading and trailing edges. The bio-inspired corrugated airfoil and the flat plate are made of wood plates with a thickness of 4.0 mm. The maximum effective thickness of the corrugated airfoil (i.e., the airfoil shape formed by fitting a spline through the protruding corners of the corrugated cross-section) is about 15% of the chord length, which is the same as the maximum thickness of the smooth-surfaced airfoil (i.e., profiled airfoil). The bio-inspired corrugated airfoil, the profiled

airfoil and the flat plate have the same chord length, i.e., $C = 101$ mm. The flow velocity at the inlet of the test section was changed from 7.0 m/s to 15.0 m/s for the present study, which corresponds to a chord Reynolds number changing from 58,000 to 125,000. The turbulence intensity of the incoming streams at the inlet of the test section was found to be within 1.0%, measured by using a hot-wire anemometer. During the experiments, the test airfoil models are mounted tightly, no obvious bending motion of the test models was observed.

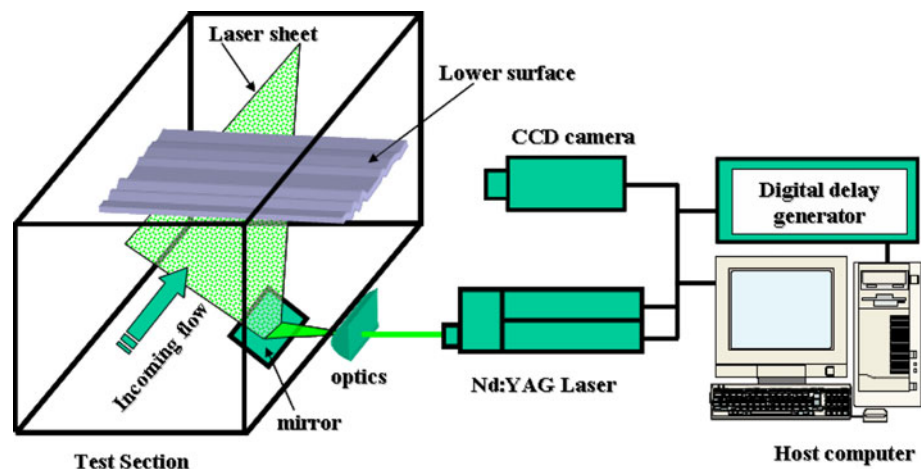
In the present study, the aerodynamic forces (lift and drag) acting on the test airfoils were measured by using a force-moment sensor cell (JR3, model 30E12A-I40) in order to determine the lift and drag coefficients ($C_L = L/(\frac{1}{2}\rho V_\infty^2 C)$; $C_D = D/(\frac{1}{2}\rho V_\infty^2 C)$) of the studied airfoils. The force-moment sensor cell is composed of foil strain gage bridges, which are capable of measuring the forces on three orthogonal axes, and the moment (torque) about each axis. The precision of the force-moment sensor cell for force measurements is $\pm 0.25\%$ of the full scale (40 N).

In addition to measuring aerodynamic forces (drag and lift) acting on the tested models, a digital PIV system was used to make detailed flowfield measurements to quantify the evolution of the unsteady vortex and turbulent structures around the tested airfoils. Figure 2 shows the experimental setup for PIV measurements. The test airfoils were installed in the middle of the test section. The PIV system was used to make flow velocity field measurements along the chord at the middle span of the airfoil models. The flow was seeded with 1–5- μm oil droplets. Illumination was provided by a double-pulsed Nd:YAG laser (NewWave Gemini 200) adjusted on the second harmonic and emitting two pulses of 200 mJ at the wavelength of 532 nm with a repetition rate of 10 Hz. The laser beam was shaped to a sheet by a set of mirrors, spherical and cylindrical lenses.

The thickness of the laser sheet in the measurement region is about 1.0 mm. A high-resolution 12-bit ($1,376 \times 1,040$ pixel) CCD camera (SensiCam-QE, CookeCorp) was used for PIV image acquisition with the axis of the camera perpendicular to the laser sheet. The CCD cameras and the double-pulsed Nd:YAG lasers were connected to a workstation (host computer) via a Digital Delay Generator (Berkeley Nucleonics, Model 565), which controlled the timing of the laser illumination and image acquisition.

Instantaneous PIV velocity vectors were obtained by a frame to frame cross-correlation technique involving successive frames of patterns of particle images in an interrogation window 32×32 pixels. An effective overlap of 50% of the interrogation windows was employed in PIV image processing. The PIV measurements were conducted at two spatial resolutions: a coarse level to study the global features of the flow fields around the airfoils with the measurement window size of about $200 \text{ mm} \times 160 \text{ mm}$; and a refined level to investigate the detailed flow structures near the leading edges of the airfoils with the measurement window size of about $50 \text{ mm} \times 40 \text{ mm}$. The effective resolutions of the PIV measurements, i.e., grid sizes, were $\Delta/C = 0.048$, and 0.012, respectively. After the instantaneous velocity vectors (u_i, v_i) were determined, instantaneous spanwise vorticity (ω_z) could be derived. The time-averaged quantities such as mean velocity (U, V), ensemble-averaged spanwise vorticity, turbulent velocity fluctuations ($\overline{u'}$, $\overline{v'}$) and normalized turbulent kinetic energy (i.e., $\text{T.K.E.} = 0.5 * (\overline{u'^2} + \overline{v'^2}) / V_\infty^2$) distributions were obtained from a cinema sequence of 500 frames of instantaneous velocity fields. The measurement uncertainty level for the velocity vectors is estimated to be within 2.0%, and that of the turbulent velocity fluctuations ($\overline{u'}$, $\overline{v'}$) and T.K.E. are about 5.0%. Further information about the experimental setup, the tested airfoils, aerodynamic force and PIV measurements is available in Murphy (2008).

Fig. 2 Experimental setup for PIV measurements



3 Experimental results and discussions

3.1 Aerodynamic force measurement results

Figure 3 shows the aerodynamic force measurement results in the terms of lift and drag coefficients of the studied airfoils as the angles of attack (AOA) of the airfoils

changed from 0.0 to 20.0 degrees and Reynolds numbers changed from 58,000 to 125,000. The measurement results of Hu and Tamai (2008) at $Re_c = 34,000$ were also given in the figures for comparison.

As shown in Fig. 3, for the flat plate, while the lift coefficient was found to increase almost linearly with the increasing angle of attack, the drag coefficient was found to

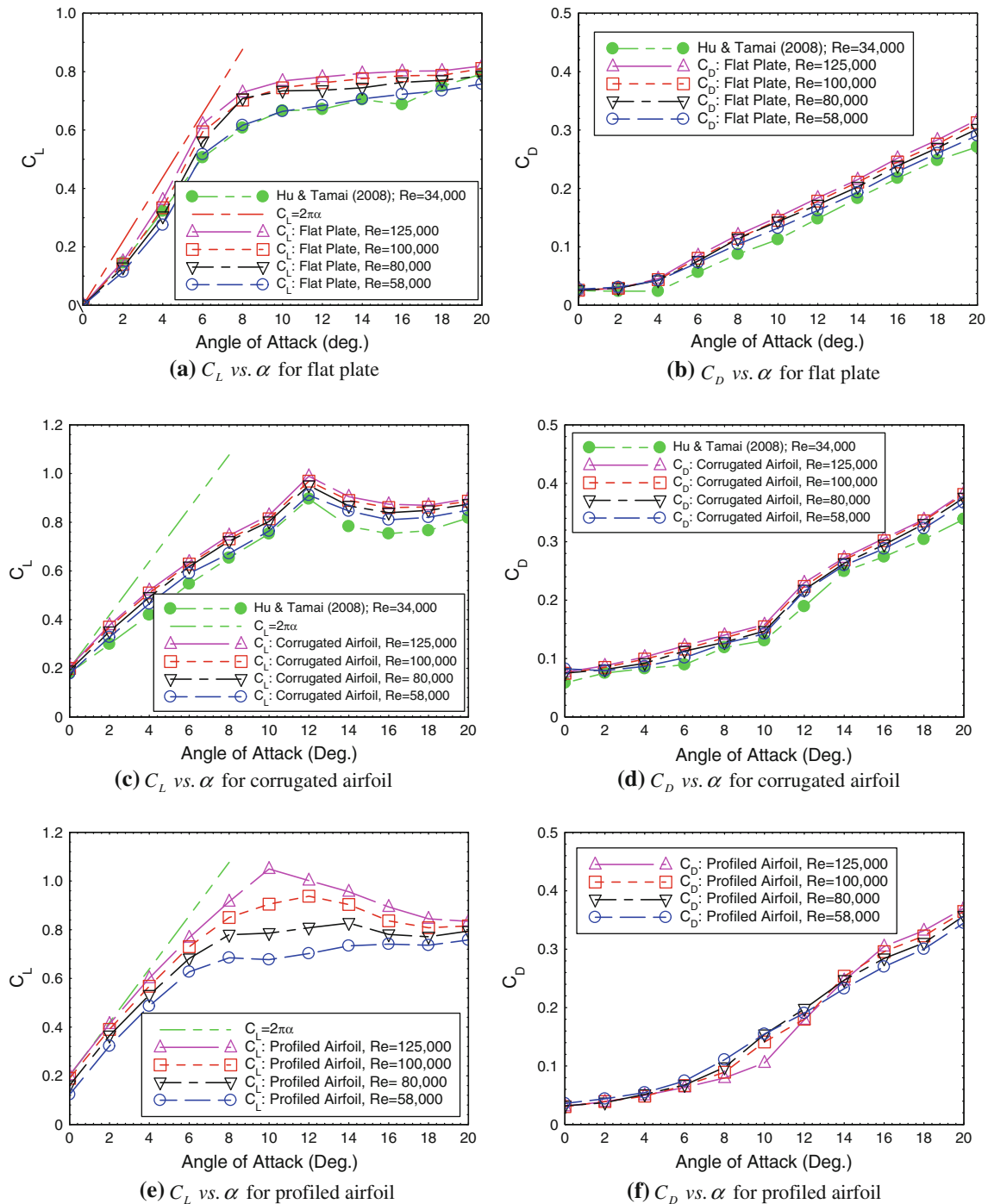


Fig. 3 Measured aerodynamic lift and drag coefficients of the tested airfoils

be reasonably small when the angle of attack is relatively low ($AOA < 6.0$ degrees). As the angle of attack becomes relatively high (i.e., $AOA > 6.0$ degrees), the increasing rates of the lift coefficient profiles were found to decrease significantly and almost flatten out. The drag coefficients of the flat plate were found to increase rapidly at $AOA > 6.0$ degrees. Such measurement results indicate that stall would occur at $AOA \approx 8.0$ for the flat plate, which was confirmed from the PIV measurement results to be discussed later. The measurement results also revealed that the lift coefficient of the flat plate would increase slightly with the increasing Reynolds number. The increase rates of the lift coefficient profiles at relatively low angles of attack were also found to increase with the increasing Reynolds number, approaching the theoretical prediction values based on inviscid thin airfoil theory (i.e., $dC_L/d\alpha = 2\pi\alpha$) at relatively high Reynolds numbers (i.e., $Re_C = 125,000$). As it is expected, the drag coefficient of the flat plate was also found to increase slightly with the increasing Reynolds numbers.

The lift coefficient of the corrugated airfoil was found to increase almost linearly with the increasing angle of attack and reach its peak value at $AOA \approx 12.0$ degrees at all the tested Reynolds number levels. Then, the lift coefficient of the corrugated airfoil was found to decrease with the increasing angle of attack at $AOA > 12.0$ degrees. The drag coefficient of the corrugated airfoil was found to increase slightly with the increasing angle of attack when the angle of attack is relatively small (i.e., $AOA < 10.0$ degrees). Then, the increasing rates of the drag coefficient profiles were found to become much more significant at $AOA > 12.0$ degrees. Such measurement results indicate that stall would take place at $AOA \approx 12.0$ degrees for the corrugated airfoil, which was confirmed from the PIV measurement results to be discussed later. It was also found that, for the corrugated airfoil, the increasing rate of the lift coefficients at relatively small angles of attack was found to be much smaller than that of the prediction based on thin airfoil theory (i.e., $dC_L/d\alpha = 2\pi\alpha$). The measurement results also revealed clearly that the Reynolds numbers have almost no effects on the aerodynamic performance (i.e., both lift and drag coefficient profiles) of the corrugated airfoil.

Although the profiled airfoil was formed simply by tautly wrapping a thin film around the corrugated airfoil, the aerodynamic performance of the profiled airfoil was found to be significantly different from that of the corrugated airfoil. When the Reynolds numbers is relatively low (i.e., $Re_C = 58,000$), the lift coefficient of the profiled airfoil was found to increase linearly at first with the increasing angle of attack at $AOA < 8.0$ degrees, and then flatten out at relatively high angle of attack (i.e., $AOA > 8.0$ degrees), which is quite similar as that of the

thin flat plate. As the Reynolds numbers increase, the linearly increasing region of the lift coefficient profiles at relatively small angles of attack was found to become wider and wider. When the Reynolds numbers become relatively high (i.e., $Re_C = 125,000$), the lift coefficient of the profiled airfoil was found to reach its maximum value at $AOA \approx 10.0$ degrees, then started to decrease with the increasing angle of attack, which is a typical behavior of a smooth-surfaced airfoil at relatively high Reynolds numbers. The increase rates of the lift coefficient profiles of the profiled airfoil at relatively low angles of attack were also found to increase with the increasing Reynolds number, approaching the theoretical prediction values based on inviscid thin airfoil theory (i.e., $dC_L/d\alpha = 2\pi\alpha$), as it is expected.

In order to make more clear comparisons, the measured lift and drag coefficients of the three studied airfoils at two tested Reynolds number levels were plotted in Fig. 4. It can be seen clearly that, at relatively low Reynolds number (i.e., $Re_C = 58,000$), the corrugated airfoil was found to have the highest lift coefficient among the three tested airfoils. As it is expected, the thin flat plate was found to have the smallest drag coefficient. While the profiled airfoil and flat plate would stall at $AOA \approx 8.0$ degrees, the airfoil stall for the corrugated airfoil was found to be delayed up to $AOA \approx 12.0$ degrees. Such measurement results indicate clearly that the corrugated airfoil could delay the airfoil stall compared with the profiled airfoil and flat plate at relatively low Reynolds numbers. This result is found to agree with the findings of Rudolph (1977), Okamoto et al. (1996), Wakeling and Ellington (1997) and Kesel (2000), who conducted the measurements at much lower Reynolds number levels ($Re_C = 700$ – $10,000$) in order to understand the fundamental physics of dragonfly flight aerodynamics.

As described above, while the aerodynamic performance of the corrugated airfoil is almost insensitive to the Reynolds numbers, the aerodynamic performance of the profiled airfoil was found to be improved greatly with the increasing Reynolds numbers. As a result, the profiled airfoil was found to have better aerodynamic performance (i.e., higher maximum lift coefficients and smaller drag coefficients) compared with corrugated airfoil when the Reynolds number becomes relatively high (i.e., $Re_C = 125,000$). The “switch over” of the higher maximum lift coefficient between the corrugated airfoil and profiled airfoil was found to take place at $Re_C \approx 100,000$. Such aerodynamic force measurement results indicate that the corrugation feature found in dragonfly wings can bring aerodynamic benefits (i.e., higher maximum lift coefficient) only for the low Reynolds number applications with chord Reynolds number $Re_C < 100,000$.

It should be noted that the corrugated airfoil was found to have relatively big drag coefficients compared with

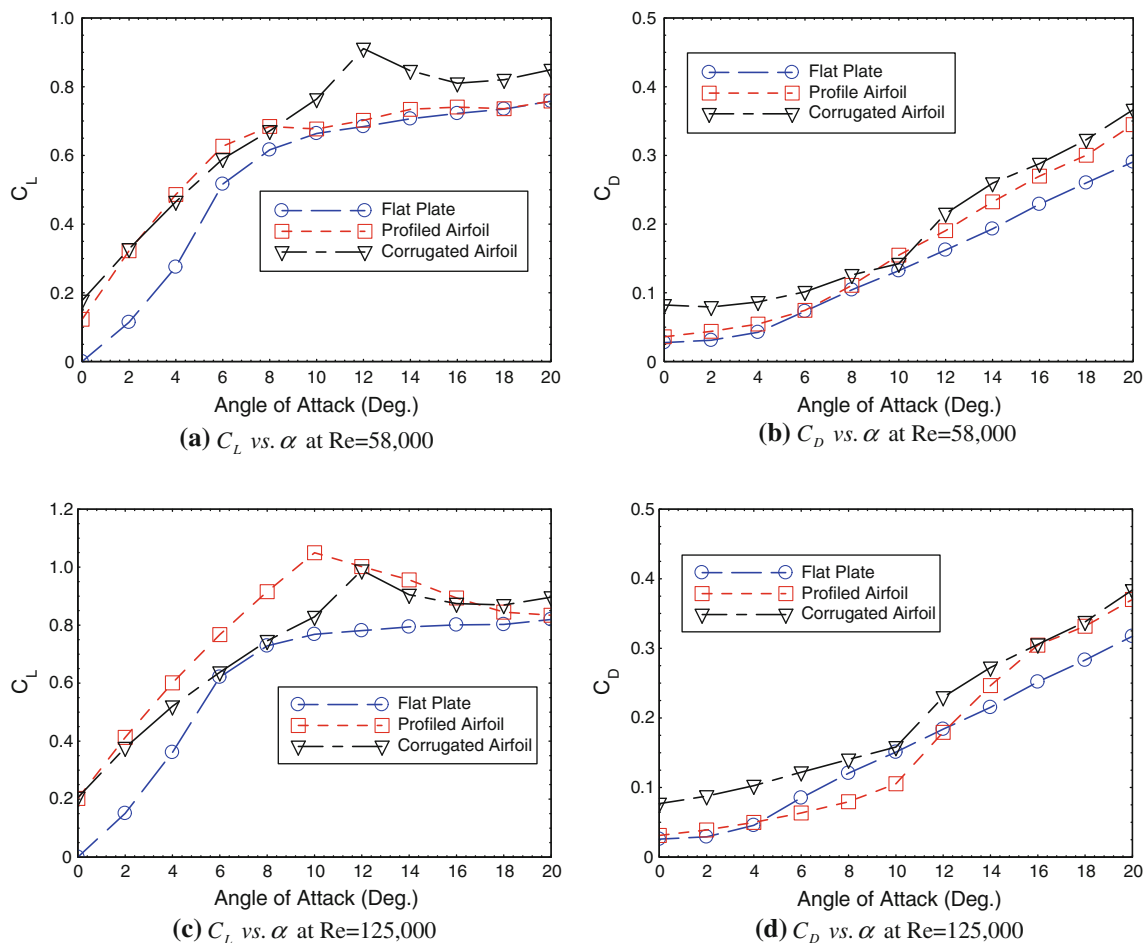


Fig. 4 The comparisons of the aerodynamic performances of the three tested airfoils

those of the smooth-surfaced airfoil and the flat plate at low angles of attack (i.e., $AOA < 8.0$ degrees). This may be an issue to limit the applications of bio-inspired corrugated airfoils, especially for the MAVs flying at low angles of attack. The corrugated airfoil was found to have comparable drag coefficients as the profiled airfoil, while maintaining a higher lift coefficient, at relatively high angles of attack (i.e., $AOA > 10$ degrees) for the low Reynolds number applications of $Re_C < 100,000$. It suggests that the unique feature of the corrugated airfoil in preventing large-scale flow separations and airfoil stall can be leveraged in MAV designs to improve their flight agility and maneuverability at relatively high angles of attack.

3.2 PIV measurement results

With the findings derived from the aerodynamic force measurements in mind, PIV measurements were carried out to visualize the transient behavior of vortex and turbulent flow structures around the three tested airfoils in order to elucidate the underlying fundamental physics associated

with the airfoil aerodynamic performance characteristics revealed from the aerodynamic force measurements.

Figure 5 shows the typical instantaneous and ensemble-averaged flow velocity fields around the tested airfoils at $AOA = 6.0$ degrees with the Reynolds number $Re_C = 58,000$. For the flat plate, as revealed clearly from the PIV measurement results given in Fig. 5A, incoming fluid streams were found to separate from the surface of the flat plate right from the leading edge, and then, reattach to the upper surface of the flat plate at the rear portion of the flat plate, i.e., a separation bubble was found to form on the upper surface near the leading edge of the flat plate. Due to the reattachment of the separated fluid streams, no apparent flow separation or large recirculation region was found in the wake of the flat plate.

As shown in the PIV measurement results given in Fig. 5B, incoming flow streams were found to flow smoothly along the upper surfaces of the profiled airfoil. Because the incoming flow streams could flow smoothly to follow the streamlined surfaces of the profiled airfoil at $AOA = 6.0$ degrees, they left the airfoil trailing edge

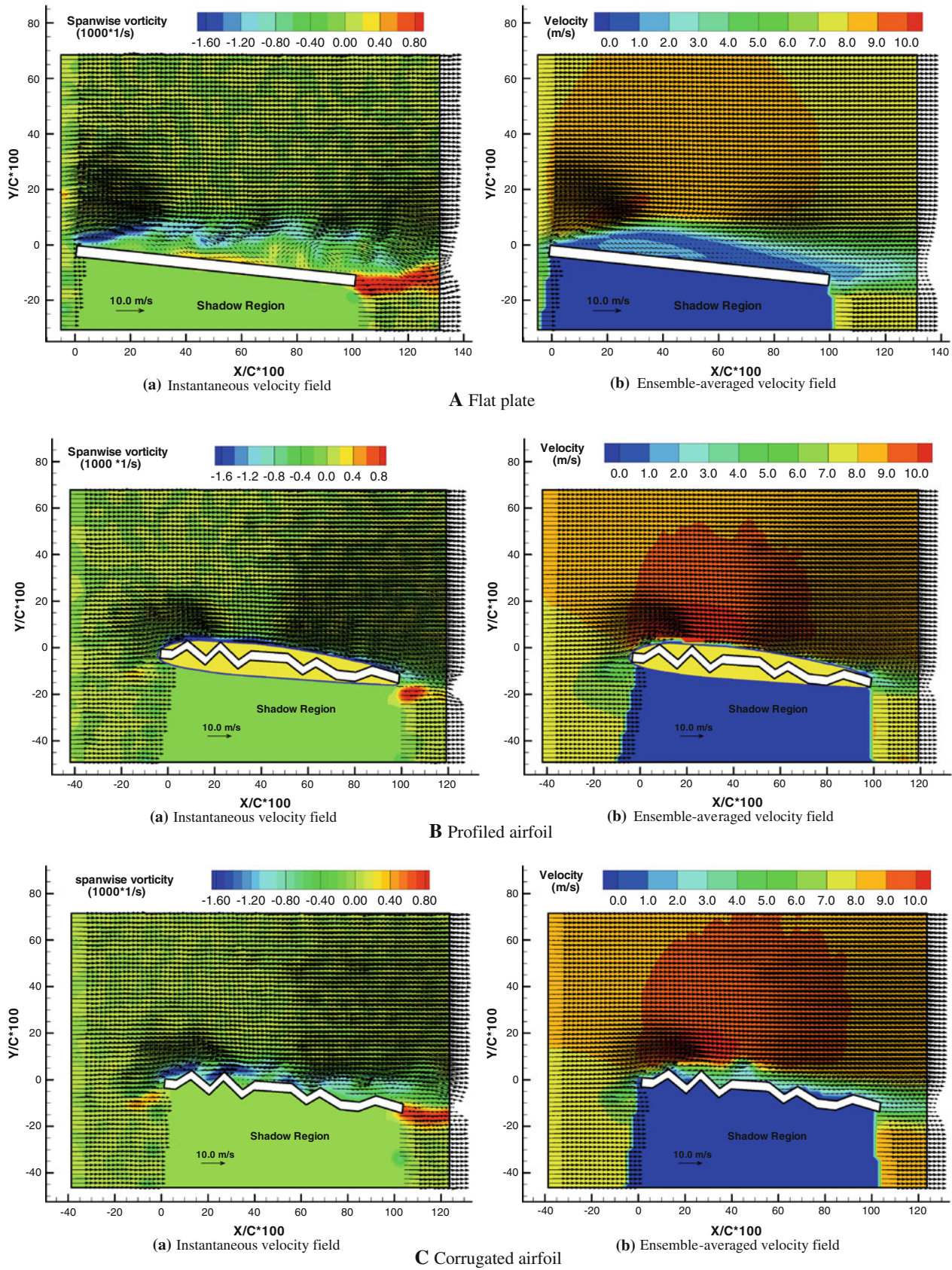


Fig. 5 PIV measurement results with AOA = 6.0 (Re = 58,000)

smoothly, which resulted in a relatively small wake region (i.e., the region with velocity deficits) downstream of the airfoil. The small wake region downstream of the airfoil would indicate a small aerodynamic drag force acting on the airfoil, which was confirmed from the aerodynamic force measurements given in Fig. 3.

For the corrugated airfoil, the existence of small circulation bubbles sitting in the valleys of the corrugation cross-section of the airfoil can be seen clearly from the measurement results given in Fig. 5C (enlarged views are given later). High-speed flow streams outside the corrugation valleys were found to flow smoothly along a virtual “envelope” profile constructed by fitting a spline through the protruding corners of the corrugated cross-section (i.e., a smooth shape formed by tautly wrapping a thin film around the corrugated airfoil). No apparent large-scale flow separation or circulation region could be found in the wake of the corrugated airfoil at $AOA = 6.0$ degrees.

Figure 6 shows the PIV measurement results when the angle of attack of the airfoils increases to 12.0 degrees. For the flat plate, the circulation bubble on the upper surface near the leading edge was found to burst when the angle of attack increased to 12.0 degrees. The high-speed flow streams separated from the upper surface at the leading edge of the flat plate could no longer reattach to the upper surface of the flat plate. Large-scale flow separation was found to occur on entire upper surface of the flat plate (i.e., airfoil stall) due to more severe adverse pressure gradient at 12.0 degrees angle of attack. The large-scale flow separation on the upper surface of the airfoil can also be seen clearly from the ensemble-averaged PIV measurement results in the form of a large recirculation bubble sitting on the flat plate. Because of the flow separation, the size of the wake region (i.e., the region with velocity deficits) downstream of the flat plate was found to be increased greatly, which indicates an increased aerodynamic drag force acting on the flat plate. The increased aerodynamic drag acting on the flat plate at $AOA = 12.0$ degrees was confirmed quantitatively for the measured drag-coefficient data given in Fig. 3.

As shown in the results given in Fig. 6B, incoming flows streams were found to flow smoothly along the streamlined nose of the profiled airfoil, as expected. However, large-scale flow separation was found to take place at most portion of the airfoil upper surface at $AOA = 12.0$ degrees due to the severe adverse pressure gradient at $AOA = 12.0$ degrees. Such flow pattern indicates that profiled airfoil was in stall state, resulting in a large circulation region in the wake of the profiled airfoil. The large deficit of the velocity profile in the wake of the profiled airfoil would indicate a rapid increase in the aerodynamic drag force acting on the airfoil due to the airfoil stall, which was also confirmed from the drag force measurement data given in

Fig. 3. However, for the corrugated airfoil, high-speed fluid streams were still found to follow the “envelope” profile of the corrugated cross-section faithfully, as revealed clearly from the PIV results given in Fig. 6C. No large-scale flow separation could be found over the upper surface of the corrugated airfoil at $AOA = 12.0$ degrees.

The adverse pressure gradient over the upper surface of the airfoils would become more and more severe as the angle of attack increased. Compared with those at $AOA = 12.0$ degrees, the circulation regions in the wakes of the profiled airfoil and the flat plate were found to be enlarged significantly when the angle of attack increased to 14.0 degrees (Fig. 7A, B), which would indicate increased aerodynamic drag forces acting on the airfoils. Because of the severe adverse pressure gradient at $AOA = 14.0$ degrees, high-speed flow streams around the corrugated airfoil were found not to be able to follow the “envelope” profile of the corrugated cross-section any longer. Large-scale flow separation was found to occur on upper surface of the corrugated airfoil (Fig. 7C), i.e., airfoil stall was also found for the corrugated airfoil at $AOA = 14.0$ degrees, which confirmed the aerodynamic force measurement data given in Fig. 3.

The PIV measurement results reveal clearly that the corrugated airfoil could delay large-scale flow separation and airfoil stall to a much higher angle of attack (up to about 12.0 degrees) compared with the profiled airfoil (airfoil stall at $AOA \approx 8.0$ degrees) and the flat plate (airfoil stall at $AOA \approx 6.0$ degrees) at low Reynolds numbers of $Re_C = 58,000$. In order to elucidate the fundamental mechanism why corrugated airfoils have better performance in preventing large-scale flow separation and delaying airfoil stall compared with the profiled airfoil and flat plates at low Reynolds numbers, refined PIV measurements near the leading edges of the airfoils were made to investigate detailed flow structures around the leading edges of the airfoils. The refined PIV measurement results are given in Figs. 8 and 9.

As described in the review articles of Carmichael (1981), Lissaman (1983) and Gad-el-Hak (2001), for smooth-surfaced airfoils at low Reynolds numbers, the boundary layers would remain laminar at the onset of the pressure recovery unless artificially tripped. Laminar boundary layers are unable to withstand any significant severe adverse pressure gradient. Therefore, the aerodynamic performances of smooth-surfaced airfoils at low Reynolds numbers are entirely dictated by the relatively poor separation resistance of the laminar boundary layers. The laminar boundary layer over the profiled airfoil was visualized clearly as a thin vortex layer over the nose of the airfoil in the instantaneous vorticity distribution given in Fig. 8. As indicated in the PIV measurement results, the laminar boundary layer would separate from the upper

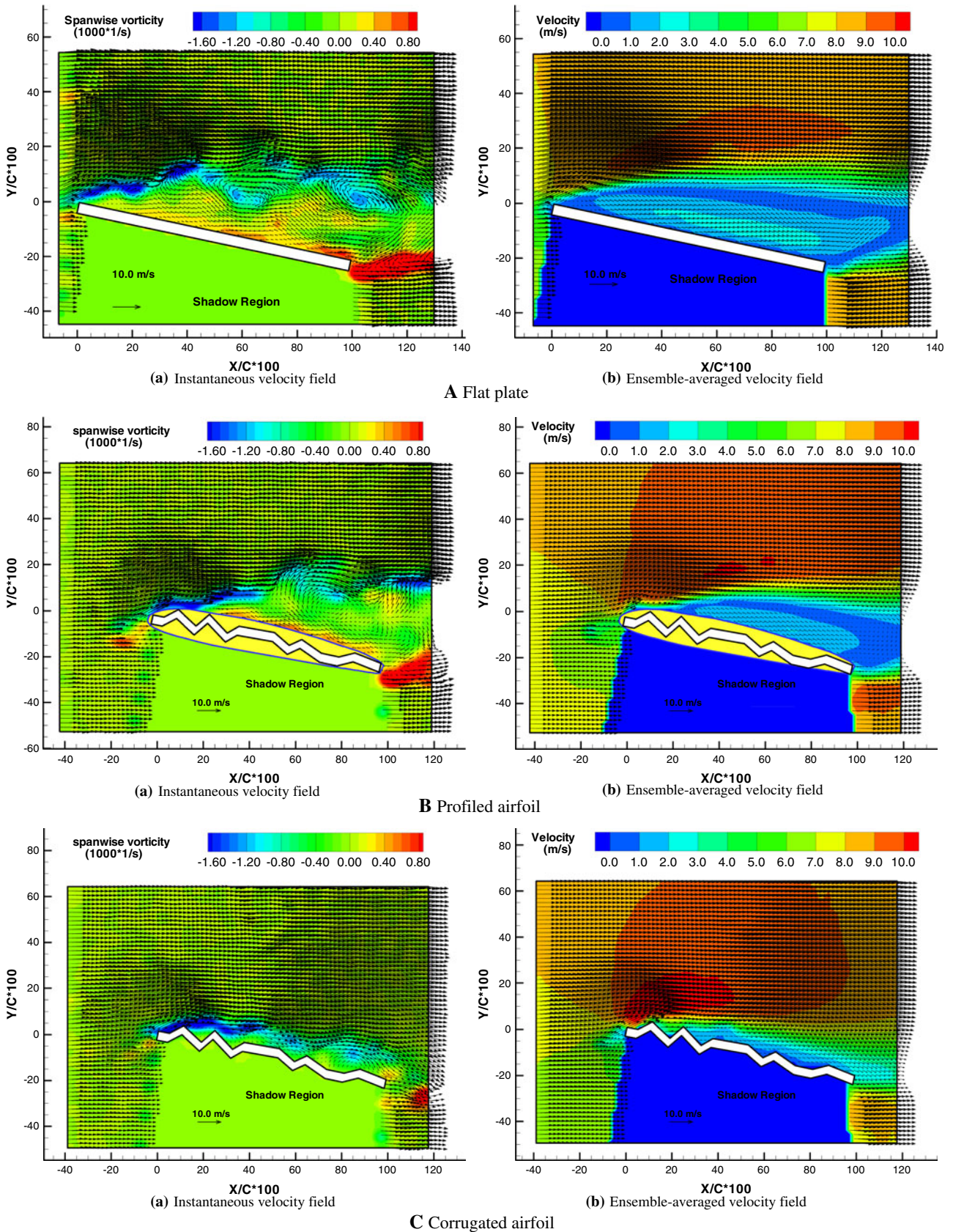


Fig. 6 PIV measurement results with AOA = 12.0 (Re = 58,000)

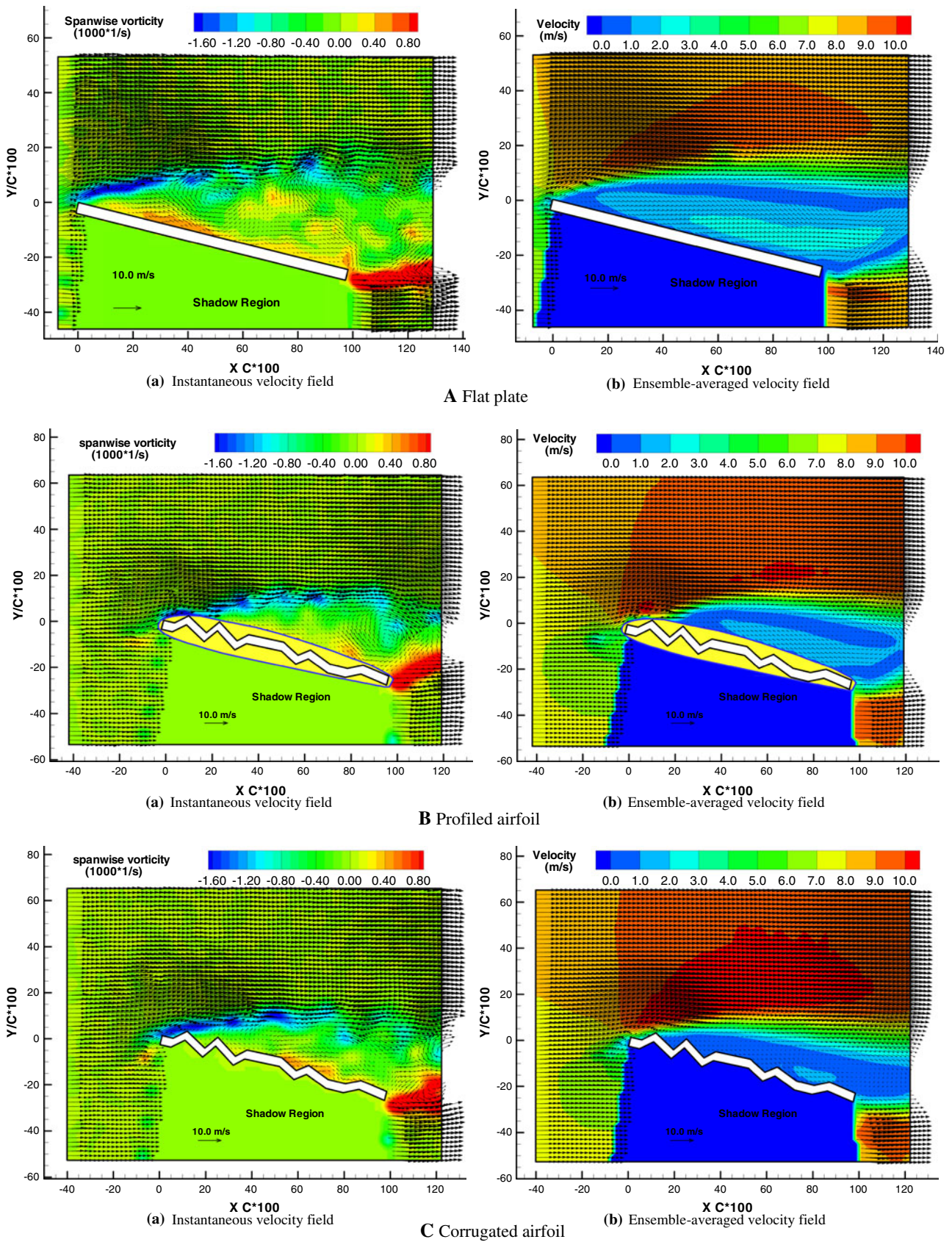


Fig. 7 PIV measurement results with AOA = 14.0 (Re = 58,000)

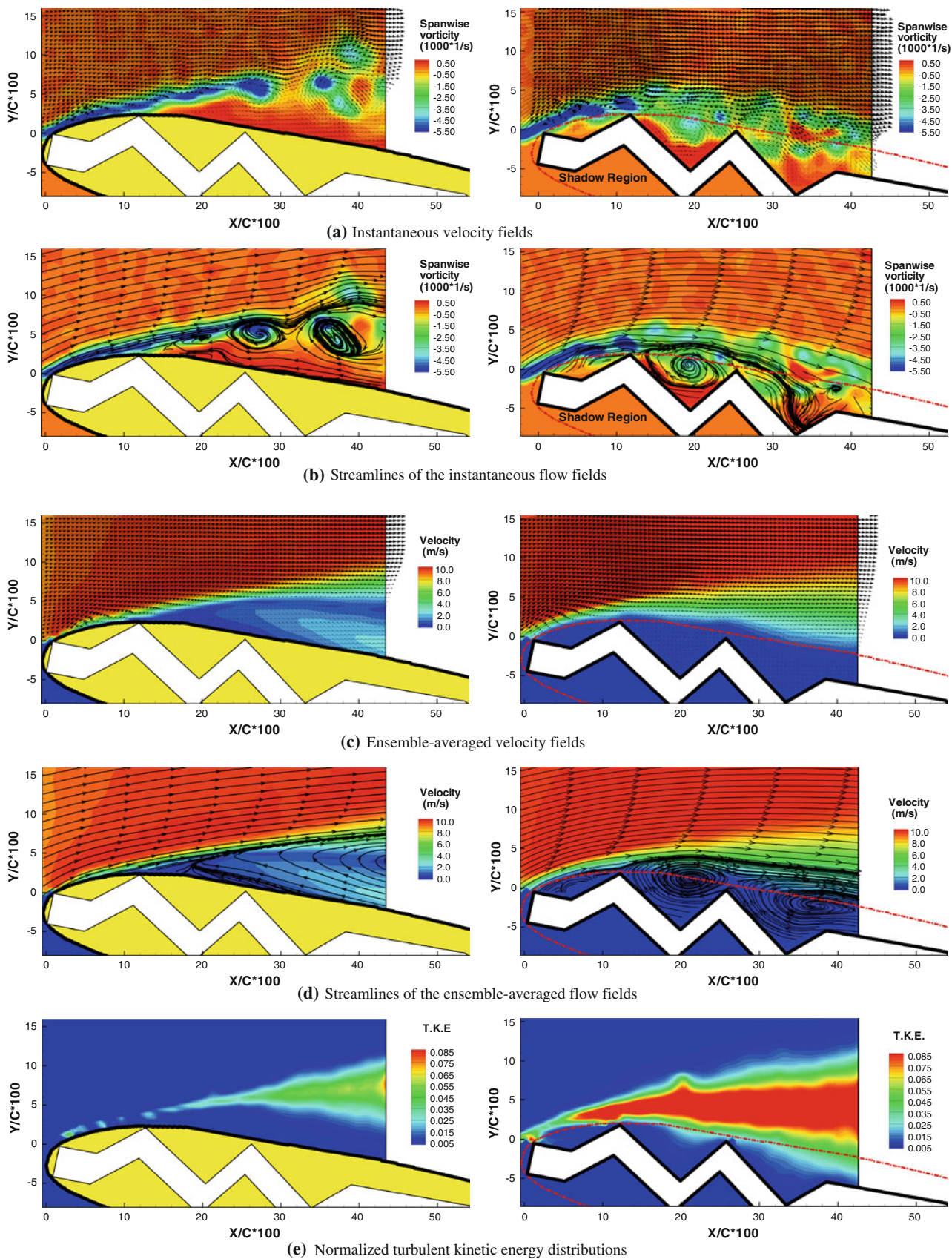


Fig. 8 Refined PIV measurements with AOA = 12.0 (Re = 58,000)

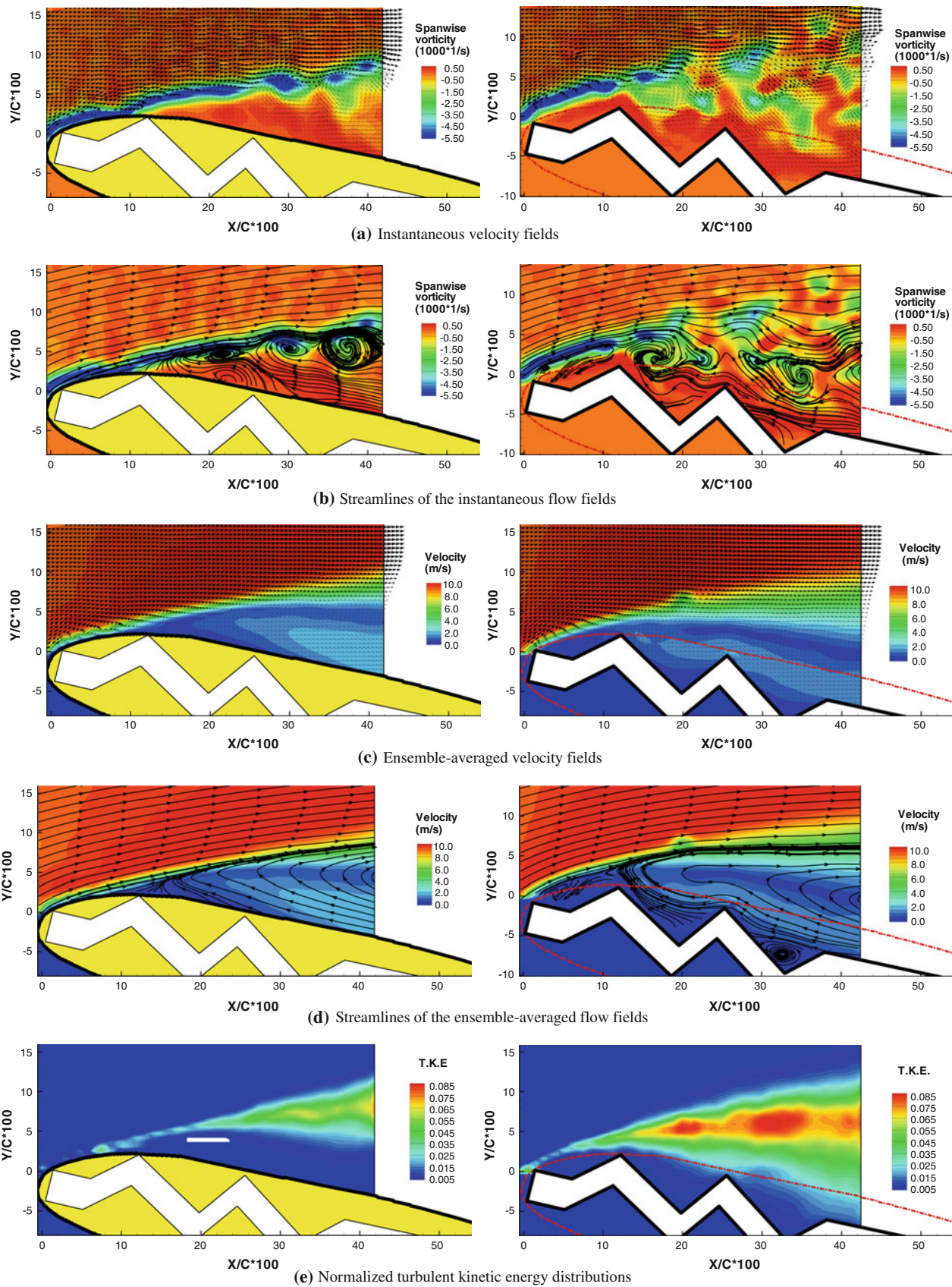


Fig. 9 Refined PIV measurements with AOA = 14.0 (Re = 58,000)

surface of the profiled airfoil at $AOA = 12$ degrees since the laminar boundary layer has very poor capacity to overcome the adverse pressure gradient. The separated laminar boundary layer would behave more like a free shear layer, which is highly unstable; therefore, rolling-up of Kelvin–Helmholtz vortex structures and transition to turbulence would be readily realized (Hu and Yang 2008). Because of the laminar nature of the boundary layer flow around the nose of the smooth-surfaced airfoil, the regions with higher turbulent kinetic energy (T.K.E.) were found to be confined within the thin separated shear layer until the separated laminar boundary layer transitioned to turbulence further downstream.

Flow around the leading edge of the corrugated airfoil was found to be much more involved than that of the profiled airfoil. As visualized clearly in the PIV measurement results given in Fig. 8, due to the sharp leading edge, incoming fluid streams were found to separate from the corrugated airfoil right from the sharp leading edge to form a laminar shear layer at first. Then, the separated laminar boundary layer was found to transition to turbulent rapidly as it approached the first protruding corner of the corrugated airfoil. Unsteady vortices were found to shed periodically from the protruding corners of the corrugated cross-section, i.e., the protruding corners of the corrugated airfoil seem to act as “turbulators” to generate unsteady vortex structures that promote the transition of the separated boundary layer from laminar to turbulent. For the profiled airfoil at the same angle of attack of $AOA = 12$ degrees, the turbulent transition and the generation of the unsteady vortex structures were found to take place in the regions relatively far away from the surfaces of the airfoils. For the corrugated airfoil, the turbulent transition and the generation of the unsteady vortex structures were found to take place in the region quite close to the protruding corners of the corrugated airfoil. Furthermore, the unsteady vortex structures were found to be trapped in the valleys of the corrugated cross-section, which would interact with the high-speed flow streams outside the valleys dynamically. Due to the interaction between the unsteady vortex structures in the corrugations valleys and outside high-speed fluid streams, high-speed fluid was found to be pumped from outside to near-wall regions (the pumping effect of the unsteady vortex structures to move high-speed fluid from outside to near-wall regions can be seen clearly from the animations of the time sequence of instantaneous PIV measurements). The pumping of high-speed fluid to near-wall regions provided sufficient kinetic energy for the boundary layer to overcome the adverse pressure gradient to suppress large-scale flow separation and airfoil stall. The mean velocity vectors and corresponding streamlines revealed clearly that small circulation bubbles would be formed in the valleys of the corrugated airfoil. High-speed

fluid streams outside the valleys would flow smoothly along the “envelope” profile of the corrugated cross-section (i.e., the dashed profile given in the figures). The rotation direction of the circulation bubbles in the valleys was found to be clockwise (flow moving from left to right) to accommodate the high-speed fluid streams outside the valleys. For the corrugated airfoil, the rapid transition of the boundary layer from laminar to turbulent due to the effect of the protruding corners as “turbulators” could also be seen clearly from the measured T.K.E. distribution, which resulted in a much higher T.K.E. level in the near-wall regions.

It should be noted that Vargas et al. (2008) conducted a numerical study to investigate flow structures around a similar corrugated airfoil as the one used in the present study, but at a much lower Reynolds number level of $Re_c = 10,000$. Despite the difference in Reynolds number of the two studies, the measurement results of the present study were found to agree well with the numerical simulation of Vargas et al. (2008) in revealing the global pattern of the flow field around the corrugated airfoil and the small vortex structures trapped in the valleys of the corrugated cross-section.

Compared with those of the smooth-surfaced airfoil (i.e., profiled airfoil), the “energetic” turbulent boundary layer over the upper surface of the corrugated airfoil would be much more capable of advancing against adverse pressure gradient to suppress flow separation. Therefore, flow streams would still be able to attach to the “envelope” profile of the corrugated airfoil faithfully even at much larger angle of attack (up to $AOA = 12.0$ degrees), while the large-scale flow separation and airfoil stall had already been found to take place for smooth-surfaced airfoil (i.e., profiled airfoil), as revealed in the PIV measurement results given in Figs. 6 and 8.

As shown in Fig. 9, although the separated laminar boundary layer over the upper surface of the corrugated airfoil was found still to transition to turbulence rapidly by generating unsteady Kelvin–Helmholtz vortex structures in the flow field when the angle of attack increases to $AOA = 14.0$ degrees, the shedding path of the unsteady vortex structures was found to be relatively far away from the surface of the corrugated airfoil. The unsteady vortex structures could no longer be trapped in the valleys of the corrugations. The ensemble-averaged velocity field and the corresponding streamlines also show clearly that the high-speed flow streams permanently separate from the upper surface of the airfoil. Although smaller circulation bubbles were still found to sit in the valleys of the corrugated cross-section, they became much weaker (i.e., much lower rotating velocity as revealed from the velocity distributions), and their rotating direction was also found to be reversed to accommodate the reversed flow outside the

valleys. The adverse pressure gradient over the upper surfaces of the airfoils would become much more significant as the angle of attack increased to $AOA = 14.0$ degrees, which requires a much more energetic boundary layer to overcome the adverse pressure gradient over the upper surface of the airfoil. However, the measured T.K.E. distribution reveals that the regions with higher turbulent kinetic energy were along the shedding path of the Kelvin–Helmholtz vortex structures, which is quite far from the surface of the corrugated airfoil. Therefore, large-scale flow separation and airfoil stall were found to take place on the corrugated airfoil due to the lack of enough kinetic energy in the boundary layer to overcome the significant adverse pressure gradient, which is confirmed from the aerodynamic force measurement data given in Fig. 3.

The PIV measurements may also be used to explain the characteristics of the drag coefficients of the corrugated airfoil revealed from the aerodynamic force measurement results shown in Figs. 3 and 4. As described earlier, while the corrugated airfoil was found to have relatively big drag coefficients compared with those of the smooth-surfaced airfoil at low angles of attack (i.e., $AOA < 8.0$ degrees), the drag coefficients of the corrugated airfoil became very comparable with those of the smooth-surfaced airfoil as the angle of attack became large enough ($AOA > 10.0$ degrees). This can be explained as follows: it is well known that the total drag force acting on an airfoil can be divided into friction drag and pressure drag. The friction drag is due to the shear stress acting on the surface of the airfoil. The pressure drag is due to the pressure difference around the surface of the airfoil. The pressure drag is also often referred to as the form drag, because of its strong dependence on the effective shape of the airfoil, which is usually indicated by the averaged streamline pattern around the airfoil. When the angle of attack is relatively small ($AOA < 8.0$ degrees), as revealed from the PIV measurements described above, the averaged streamline patterns around the corrugated airfoil and the smooth-surfaced airfoil are very similar (i.e., incoming streams would flow smoothly along the “envelope” profile of the airfoil without any large-scale flow separation occurring on the upper surface of the airfoil). It suggests that the pressure drags acting on the corrugated airfoil and the smooth-surfaced airfoil would be quite small and similar at relatively low angle of attack ($AOA < 8.0$ degrees). The slightly higher drag acting on the corrugated airfoil is believed to be closely related to the fact that the corrugated airfoil has a much larger contact area with moving flow streams (i.e., increased friction drag), due to its complex shape of the corrugated cross-section. As the angle of attack becomes large enough, airfoil stall takes place for the test airfoils (i.e., the flat plate and the smooth-surfaced technical airfoil at $AOA \approx 8.0$ degrees, and corrugated airfoil at

$AOA \approx 12.0$ degrees). After airfoil stall, the pressure drags increase dramatically, and the friction drags become negligible. Therefore, the drag forces acting on the airfoils are mainly determined by pressure drags, which could be indicated by the averaged streamline patterns around the airfoils. As revealed clearly in the PIV measurement results, the averaged streamline pattern for the flow around the corrugated airfoil is very much the same as those around the smooth-surfaced airfoil after airfoil stall; that is, a very large separation bubble would be generated to cover the entire upper surface of the airfoil. Therefore, the drag coefficient of the corrugated airfoil would become very comparable with those of the smooth-surfaced airfoil at relatively large angles of attack.

4 Concluding remarks

An experimental study was conducted to investigate the aerodynamic characteristics and flow features around a bio-inspired corrugated airfoil compared with a smooth-surfaced airfoil and a flat plate at chord Reynolds number of $Re_C = 58,000$ – $125,000$ to explore the potential applications of non-traditional, bio-inspired corrugated airfoils for MAV applications. The experimental study was conducted in a low-speed wind tunnel with PIV to make detailed flow field measurements in addition to total aerodynamic force measurements. The detailed flow field measurements were correlated with the aerodynamic force measurement data to elucidate underlying physics to improve our understanding about how and why the corrugation feature found in the dragonfly wings holds aerodynamic advantages for low Reynolds number flight applications. The key to designing better airfoils for improved aerodynamic performance for MAV applications is to know how to exploit the advantages of the corrugation feature and knowing its limitations.

The aerodynamic force measurements revealed that, compared with the smooth-surfaced airfoil and flat plate, the corrugated airfoil could generate higher lift and delay airfoil stall to much higher angle of attack for low Reynolds number flight applications of $Re_C < 100,000$. While aerodynamic performance of the smooth-surfaced airfoil and the flat plate would vary considerably with the changing of the Reynolds numbers, the aerodynamic performance of the corrugated airfoil was found to be almost insensitive to chord Reynolds numbers. The corrugated airfoil was found to have relatively big drag coefficients compared with those of the smooth-surfaced airfoil and the flat plate at low angles of attack (i.e., $AOA < 8.0$ degrees). This may be an issue to limit the applications of bio-inspired corrugated airfoils, especially for the MAVs flying at low angles of attack. The corrugated airfoil was found to have very comparable drag coefficients as the

smooth-surfaced airfoil, while maintaining a higher lift coefficient, at relatively high angles of attack (i.e., AOA > 10 degrees) for the low Reynolds number applications of $Re_C < 100,000$. It suggests that the unique feature of the corrugated airfoil in preventing large-scale flow separations and airfoil stall can be leveraged in MAV designs to improve their flight agility and maneuverability at relatively high angles of attack.

The detailed PIV measurements elucidated underlying physics about how and why corrugated airfoils could suppress large-scale flow separation and airfoil stall at low Reynolds numbers. It was found that the protruding corrugation corners would act as boundary layer trips to promote the transition of the boundary layer from laminar to turbulent while remaining ‘attached’ to the envelope profile of the high-speed streamlines. The valleys of the corrugated cross-section of the airfoil would trap unsteady vortex structures that help the boundary layer become more energetic and stay ‘attached’ by pulling high-speed flow into near-wall regions. It is by these two processes that the corrugated airfoil can provide sufficient kinetic energy within the boundary layer flow to overcome the adverse pressure gradient, thus discourage large-scale flow separation and delay airfoil stall to much higher angle of attack.

It should be noted that the geometric parameters of the corrugated-airfoil model used in the present study were chosen rather arbitrarily. Further systematic studies are needed to explore/optimize such bio-inspired airfoil shape and wing planform design paradigms (i.e., the effects of the design parameters such as the geometry of the corrugated profile, the camber of the airfoil, the thickness of the airfoil, the stiffness of the material or flexibility of the airfoil, the corner sharpness of the corrugations, etc.) to achieve improved aerodynamic performance for MAV applications.

Acknowledgments The authors want to thank Mr. Bill Rickard of Iowa State University for his help in conducting the experiments. The support of National Science Foundation CAREER program under award number of CTS-0545918 is gratefully acknowledged.

References

- Azuma A, Watanabe T (1988) Flight performance of a dragonfly. *J Exp Biol* 137:221–252
- Carmichael BH (1981) Low Reynolds number airfoil survey. 1 NASA CR-165803
- Gad-el-Hak M (2001) Micro-air-vehicles: can they be controlled better. *J Aircr* 38(3):419–429
- Hu H, Tamai M (2008) A bio-inspired corrugated airfoil at low Reynolds numbers. *J Aircr* 47(6):2068–2077
- Hu H, Yang Z (2008) An experimental study of the laminar flow separation on a low-Reynolds-number airfoil. *J Fluid Eng* 130(5):051101
- Kesel AB (2000) Aerodynamic characteristics of dragonfly wing sections compared with technical aerofoil. *J Exp Biol* 203:3125–3135
- Kesel AB, Philippi U, Nachtigall W (1998) Biomechanical aspects of insect wings—an analysis using the finite element method. *Comput Biol Med* 28:423–437
- Kwok R, Mittal R (2005) Experimental investigation of the aerodynamics of a modeled dragonfly wing section. AIAA region I-MA student conference, Charlottesville, Virginia, 8–9 April 2005
- Lissaman PBS (1983) Low Reynolds number airfoils. *Annu Rev Fluid Mech* 15:223–239
- Luo G, Sun M (2005) The effects of corrugation and wing planform on the aerodynamic force production of sweeping model insect wings. *Acta Mech Sinica* 21:531–541
- Mueller TJ (ed) (2001) Fixed and flapping wing aerodynamics for micro air vehicle applications. Progress in Astronautics and Aeronautics, ISBN 1-56347-517-0
- Murphy JT (2008) Experimental investigation of biomimetic wing configurations for Micro Air Vehicle applications. MS thesis. Department of Aerospace Engineering of Iowa State University
- Newman BG, Savage SB, Schouella D (1977) Model test on a wing section of an *Aeschna* dragonfly. In: Pedley TJ (ed) Scale effects in animal locomotion. Academic Press, London, pp 445–477
- Okamoto M, Yasuda K, Azuma A (1996) Aerodynamic characteristics of the wings and body of a dragonfly. *J Exp Biol* 199:281–294
- Rees CJC (1975a) Form and function in corrugated insect wings. *Nature* 256:200–203
- Rees CJC (1975b) Aerodynamic properties of an insect wing section and a smooth aerofoil compared. *Nature* 258:141–142
- Rudolph R (1977) Aerodynamic properties of *Libellula quadrimaculata* L. (Anisoptera: Libellulidae), and the flow around smooth and corrugated wing section models during gliding flight. *Odonatologica* 7:49–58
- Somps C, Luttgies M (1985) Dragonfly flight: novel uses of unsteady separation flows. *Science* 228(4705):1326–1329
- Sudo S, Tsuyuki K (2000) Wing morphology of some insects. *JSME Int J C* 43:895–900
- Thomas ALR, Taylor GK, Srygley RB, Nudds RL, Bomphrey RJ (2004) Dragonfly flight: free-flight and tethered flow visualizations reveal a diverse array of unsteady lift-generating mechanisms, controlled primarily *via* angle of attack. *J Exp Biol* 207:4299–4323
- Vargas A, Mittal R (2004) Aerodynamic performance of biological airfoils. 2nd AIAA Flow Control conference, Portland, OR, AIAA Paper 2004-2319
- Vargas A, Mittal R, Dong H (2008) A computational study of the aerodynamic performance of a dragonfly wing section in gliding flight. *Bioinspir Biomim* 3:026004. doi:10.1088/1748-3182/3/2/026004
- Wakeling JM, Ellington CP (1997) Dragonfly flight: I. Gliding flight and steady-state aerodynamic forces. *J Exp Biol* 200:543–556